Journal of Power Sources 201 (2012) 103–111

Contents lists available at SciVerse ScienceDirect

Journal of Power Sources

journal homepage: www.elsevier.com/locate/jpowsour

# Development of new anodes compatible with the solid oxide fuel cell electrolyte $BaIn_{0.3}Ti_{0.7}O_{2.85}$

F. Moser[a], M.T. Caldes[a,*], M. Benamira[a], J.M. Greneche[b], P. Leone[a], O. Joubert[a]

[a] Institut des Matériaux Jean Rouxel (IMN), Université de Nantes, CNRS, 2 Rue de la Houssinière, BP 32229, 44322 Nantes Cedex 3, France
[b] UMR 6087 CNRS - Université du Maine, Laboratoire de Physique de l'Etat Condensé, Avenue Olivier Messiaen, 72085 Le Mans Cedex, France

ARTICLE INFO

*Article history:*
Received 5 September 2011
Received in revised form 23 October 2011
Accepted 31 October 2011
Available online 6 November 2011

*Keywords:*
SOFC anodes
MIEC
Electrical conductivity
$^{57}$Fe Mössbauer spectrometry
EIS
Coking

ABSTRACT

A new family of MIEC compounds resulting from the electrolyte $BaIn_{0.3}Ti_{0.7}O_{2.85}$ (BIT07) was developed by coupled substitution of titanium by iron and barium by lanthanum. Total conductivity increases significantly with iron and lanthanum content. $BaIn_{0.3}Ti_{0.7}O_{2.85}$ yields a total conductivity in air of $10^{-2}$ S cm$^{-1}$ at 700 °C whereas that of $Ba_{0.7}La_{0.3}In_{0.3}Ti_{0.1}Fe_{0.6}O_{3-\delta}$ (BLITFe06) is 3 S cm$^{-1}$. Doped compounds are p-type conductors. In reducing atmosphere the electrical conductivity decreases drastically to $\sigma = 2 \times 10^{-2}$ S cm$^{-1}$ for the best value, which is not sufficient for a use as MIEC anode. Nevertheless, Ni/BLITFe06 cermets seem to be good candidates as SOFC anodes. The total conductivity of Ni/BLITFe cermets is higher than that of 18.7 vol.% Ni/BIT07 ($\sigma_{700\,°C} \approx 10^2$ S cm$^{-1}$), even for a lower Ni content (16.1 vol.% Ni/BLITFe $\sigma_{700\,°C} \approx 200$ S cm$^{-1}$). The percolation threshold moves towards the small quantities of nickel (from 15.7 vol.% to 10 vol.%). Ni/BLITFe06 cermets, compared with Ni/BIT07, show a better electrochemical behaviour towards fuel oxidation.



## 1. Introduction

The development of new electrolyte materials with improved properties is essential to the future of intermediate temperature solid oxide fuel cells (IT-SOFCs) technology. Several electrolytes have been described as finding practical application in SOFCs: $ZrO_2$-, $CeO_2$-, $LaGaO_3$-, and $La_{10}Si_6O_{27}$-based [1,2]. Jayaraman et al. [3] reported a new family of anionic conductors $Ba_2In_{2(1-x)}Ti_{2x}O_{5+x}\square_{1-x}$ with $0 \le x \le 0.7$ (called BITx) which can be also considered as potential electrolytes for SOFC, mainly the phase $BaIn_{0.3}Ti_{0.7}O_{2.85}$ (BIT07).

In order to design anodes chemically and mechanically compatible with BIT07 electrolytes, Ni/BIT07 cermets were prepared and characterized [4]. Authors obtained a cermet containing only 18.7 vol.% of nickel with an open porosity of 40%. Its electronic conductivity ($\sigma_{700\,°C} \approx 10^2$ S cm$^{-1}$) is higher than that of Ni/YSZ cermets with a larger nickel content and the thermal expansion coefficient measured, $11.4 \times 10^{-6}$ K$^{-1}$, is close to that of the electrolyte compound BIT07 ($9.9 \times 10^{-6}$ K$^{-1}$). The Ni/BIT07 cermet was used as anode in single-cells based on BIT07 electrolyte and using $La_{0.8}Sr_{0.2}MnO_3$ as cathode [5]. The value of $P_{max}$ at 690 °C under dry hydrogen was found to be 100 mW cm$^{-2}$ whereas that under dry natural gas was 8 mW cm$^{-2}$. Indeed, Ni-based anodes are usually unstable in the presence of hydrocarbons because Ni catalyzes the formation of coke unless large amounts of steam are also present. High currents and low concentration (4–9%) of dry $CH_4$ can also prevent coke build-up for operating temperatures less than 700 °C.

Since oxides catalyze less cracking, anodes based exclusively on ceramic mixed ionic–electronic conductors (MIECs) have been extensively studied in the literature [6–9]. However, it proved to be difficult to obtain good electronic conductivity and good catalytic activity, in the same ceramic material, even if promising properties were reported for some perovskite like $La_{1-x}Sr_xCr_{1-y}Mn_yO_{3-\delta}$ ($x = 0.2$–$0.3$; $y \le 0.5$) and $Sr_2MoMg_{1-x}Mn_xO_{6-\delta}$ [6–9]. However, the most crucial factor for these materials is a relatively low electronic conduction leading to electronic transport limitations.

On the other hand, Hamakawa et al. [10] described a Ni-based catalyst composed of a MIEC support oxide which induces a self anti-coking phenomenon during methane conversion. In fact, the self-migration of lattice oxygen inside the support like the balance between the oxide ionic and electronic conductivities, play an important role to prevent accumulation of deposited carbon over the catalysts. Consequently, another way to prepare anodes resistant to coke while preserving Ni, which exhibits excellent electrocatalytic properties, could be to use a MIEC as component of the anode, i.e. a Ni–MIEC cermet. A potential way to improve the stability of the Ni/BIT07 cermets under dry natural gas possibly will be to induce electronic conductivity into BIT07 compounds. In this work a new family of MIEC compounds derivate from BIT07 by substitution of Ti by Fe (Fe → Ti) $BaIn_{0.3}Ti_{0.7-y}Fe_yO_{3-\delta}$

* Corresponding author. Tel.: +33 2 40 37 39 36; fax: +33 2 40 37 39 95.
*E-mail address:* maite.caldes@cnrs-imn.fr (M.T. Caldes).

0378-7753/$ – see front matter © 2011 Elsevier B.V. All rights reserved.
doi:10.1016/j.jpowsour.2011.10.120

(BITFey) has been synthesized and characterized. La-derivate compounds $Ba_{1-z}La_zIn_{0.3}Ti_{0.7-y}Fe_yO_{3-\delta}$ (BLITFey) were also prepared and studied. Finally, Ni/MIEC cermets based on BLITFe phases were elaborated and investigated as potential anode material.

## 2. Experimental

$BaIn_{0.3}Ti_{0.7-y}Fe_yO_{3-\delta}$ (BITFey) compounds were synthesized by solid state reaction of $BaCO_3$, $In_2O_3$, $TiO_2$ and $Fe_2O_3$. Reactants were mixed in stoichiometric proportions, ground thoroughly in acetone and calcinated at 1200 °C for 24 h. Powders thus obtained were ground, passed through the 100 mesh sieve and uniaxially pressed into disks. Finally the samples were sintered in air at 1350 °C for 24 h. $Ba_{1-z}La_zIn_{0.3}Ti_{0.7-y}Fe_yO_{3-\delta}$ (BLITFey) compounds were prepared according to the same protocol as BITFey. $La_2O_3$ was used as precursor of lanthanum.

Ni/BLITFe06 cermets were elaborated from powders of as prepared $Ba_{0.7}La_{0.3}In_{0.3}Ti_{0.1}Fe_{0.6}O_{3-\delta}$ (grain size 100 μm) and NiO (grain size 0.5–1 μm) mixed in different BLITFe06/NiO weight ratios: 75/25, 70/30, 60/40. Both mixtures were introduced with twenty glass balls (Ø 5 mm) into a 30 mL glass vessel and then placed on a roller bank for 2 h at 30 rpm. Samples of the resulting $Ba_{0.7}La_{0.3}In_{0.3}Ti_{0.1}Fe_{0.6}O_{3-\delta}$/NiO mixture were pressed to obtain pellets of Ø 10 mm (thickness 2 mm) that were heated at 1200 °C for 6 h in order to get a porous matrix, while minimizing shrinkage.

A multilayer tape casting and co-sintering processes were used for fabricating Ni/BIT07//BIT07//Ni/BIT07 and Ni/BLITFe06//BIT07//Ni/BLITFe06 symmetrical cells. The slurries for tape casting process were prepared by a ball milling process including two steps. In the first step, ceramic powders of BIT07 and of cermets were milled in a planetary mill for 1 h using zirconia balls as milling medium with ethanol and 2-butanone as the solvents, and oleic acid as dispersant. Secondly, polyvinyl butyral (PVB) and polyethylene glycol (PEG) used as binder and plasticizer, respectively, were added, then milled for another 24 h. Before tape casting, the slurries were deaerated for 24 h using a roller bank.

The cermet film was cast first onto the glass plate by a "doctor blade" method and dried in air for several minutes; then BIT07 electrolyte and cathode substrate were cast on top of the tape. After drying overnight at room temperature, the multilayer tape was detached, waiting for co-sintering. The multilayer tape was co-sintered at 1300 °C during 6 h and circular symmetrical cells (diameter 10–13 mm) were cut.

X-ray powder diffraction (XRD) patterns of all materials were recorded using a Brüker "D8 Advance" powder diffractometer operated in Bragg–Brentano reflection geometry with a Cu anode X-ray source, a focusing Ge(1 1 1) primary monochromator (selecting the Cu $K\alpha_1$ radiation) and a 1-D position-sensitive detector ("Vantec" detector). Refinements of cell parameters were carried out using the program FULLPROF [11]. Thermal expansion coefficient (TEC) was inferred from X-ray diffraction patterns recorded from room temperature up to 1000 °C.

The temperature-programmed reduction (TPR) studies were performed in a chemisorption unit Micromeritics AutoChem 2910 using powdered samples of 100 mg. Before reaction, samples were treated with helium at 300 °C for 10 min and cooled to room temperature. The TPR experiments were carried out under a 5.1% $H_2$/Ar mixture flowed through the sample at 50 mL $min^{-1}$, raising the temperature at 10 °C $min^{-1}$ up to 850 °C. The consumption of hydrogen was monitored on-line with a thermal conductivity detector.

Transmission electron microscopy (TEM) study was carried out with a Hitachi H9000NAR electron microscope, operating at 300 kV equipped with an energy dispersive X-ray (EDX) analyzer. The compounds were gently ground in ethanol and microcrystals were deposited on a holed carbon film supported by a copper grid.

$^{57}$Fe Mössbauer spectra were recorded in transmission geometry with a constant acceleration spectrometer using a room temperature $^{57}$Co(Rh) source. α-Fe foil was used at 300 K as standard to calibrate velocity and isomer shift. Powdered samples were studied at 300 K and 77 K using a cryostat. The spectra were computed with a least squares routine using quadrupolar components based on lorentzian lines.

The standard DC four-probe method was used to measure the electrical conductivity in air and under reducing atmosphere (95% Ar/5% $H_2$) between 300 °C and 800 °C. Sintered pellets densified to over 95% of theoretical density were cut to rectangular-shaped samples with dimensions 2 mm × 2 mm × 10 mm and subjected directly to electrical conductivity measurements.

Symmetrical cells were studied by electrochemical impedance spectroscopy (EIS). The measurements were carried out using a frequency response analyzer Solartron 1260. The impedance spectra were recorded over a frequency range 2 MHz to 0.01 Hz with signal amplitude of 50 mV and with 10 points per decade under open circuit conditions. A stabilisation time of one hour was considered between each temperature change.

## 3. Results and discussion

### 3.1. The iron substituted BIT07 compounds: $BaIn_{0.3}Ti_{0.7-y}Fe_yO_{3-\delta}$

The XRD patterns of $BaIn_{0.3}Ti_{0.7-y}Fe_yO_{3-\delta}$ (BITFey) compounds prepared as described in the experimental section are shown in Fig. 1(a). Single phase compounds were obtained in the composition range $0 \le y \le 0.4$. They exhibit a cubic perovskite structure which can be described in space group P*m*-3*m*. The cell parameter *a* increases weakly with increasing Fe content as illustrated in Fig. 1(b).

For $y \ge 0.5$, even if no extra peaks corresponding to secondary phases were observed in XRD patterns, the full width at half maximum (FWHM) of the diffraction peaks (e.g. see Fig. 1(b) for the (1 1 0) reflection ($2\theta \approx 31°$)) is much larger. This feature indicates a structural distortion or a biphased compound.

In order to go further in the characterization of this specific aspect, a TEM study of $BaIn_{0.3}Ti_{0.1}Fe_{0.6}O_{3-\delta}$ was performed. No secondary phase was detected. The reciprocal lattice of this compound was studied by selected area electron diffraction (SAED). No sign of amorphisation was detected. Main reflections could be indexed in the space group P*m*-3*m* (see Fig. 2(a) and (b)). However, for some zone axes (i.e. [1 1 5] in Fig. 2(c)), a phenomenon of diffuse scattering is observed, which could be due to a short range order of oxygen vacancies and/or B-site cations. Moreover, in some crystals forbidden reflections in P*m*-3*m* S.G. are observed, even if they are very diffuse, indicating a lowering of symmetry. Nevertheless, it should be noted that the stacking of the layers remains very regular, as evidenced from the [1 1 0] high resolution image illustrated in Fig. 2(d).

As will be discussed below, a mixed-valence Fe(III/IV) state occurs in these materials at room temperature, thus the aliovalent substitution of Ti(IV) by Fe(III/IV) implies the formation of charge-compensating oxygen vacancies which number increases with the iron content. For $y \ge 0.5$, the oxygen vacancies content becomes high enough to destabilize the cubic perovskite structure. This feature is translated into the XRD pattern by a broadening of the diffraction peaks.

To stabilize the cubic structure for high iron rates the substitution of Ti by Fe was coupled to that of Ba by La (La → Ba). This double substitution is expected to limit the number of charge-compensating oxygen vacancies formed during reaction and obtain a better mismatch between AO and $BO_2$ layers

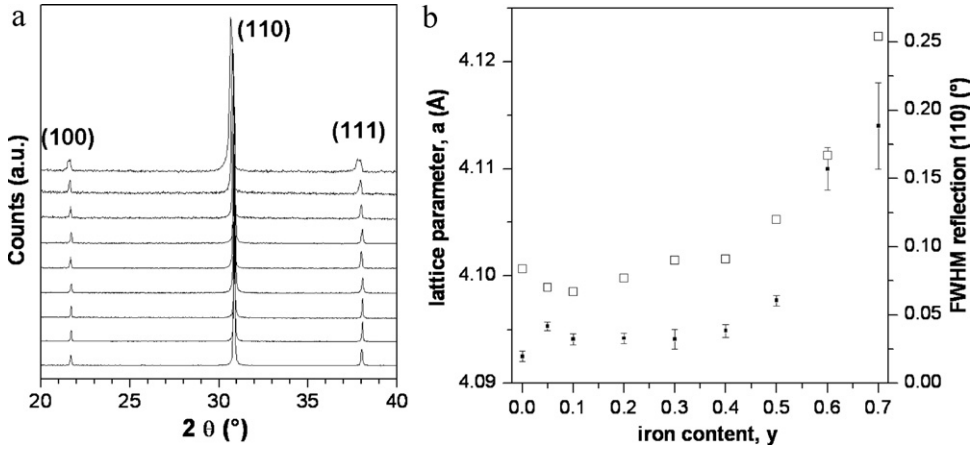


**Fig. 1.** (a) XRD patterns of $BaIn_{0.3}Ti_{0.7-y}Fe_yO_{3-\delta}$ with $0 \le y \le 0.7$ under air at RT and (b) lattice parameter and FWHM of the (1 1 0) reflection vs. Fe content.

in the perovskite structure. Thus, the La-derivate compounds $Ba_{1-z}La_zIn_{0.3}Ti_{0.7-y}Fe_yO_{3-\delta}$ ($y = 0.5$ and 0.6; $0 \le z \le 0.7$) were synthesized and then characterized.

### 3.2. The lanthanum substituted BITFey compounds: $Ba_{1-z}La_zIn_{0.3}Ti_{0.7-y}Fe_yO_{3-\delta}$

$Ba_{1-z}La_zIn_{0.3}Ti_{0.7-y}Fe_yO_{3-\delta}$ (BLITFey) compounds were prepared in a similar way that BITFey. Both substitutions Fe → Ti and La → Ba allowed to stabilize the cubic perovskite structure for high iron contents ($y = 0.6$). The XRD patterns of $Ba_{1-z}La_zIn_{0.3}Ti_{0.1}Fe_{0.6}O_{3-\delta}$ compounds ($0 \le z \le 0.7$) are shown in Fig. 3(a).

As illustrated in Fig. 3(b), for the composition range $0 \le z \le 0.2$, the FWHM of the diffraction peaks decreases with increasing La content. For $0.2 \le z \le 0.5$ the reflection width is narrow enough to refine lattice parameters in the cubic P*m*-3*m* SG. As expected, the replacement of $Ba^{2+}$ (effective ionic radius: $r_e = 1.42$ Å) by smaller

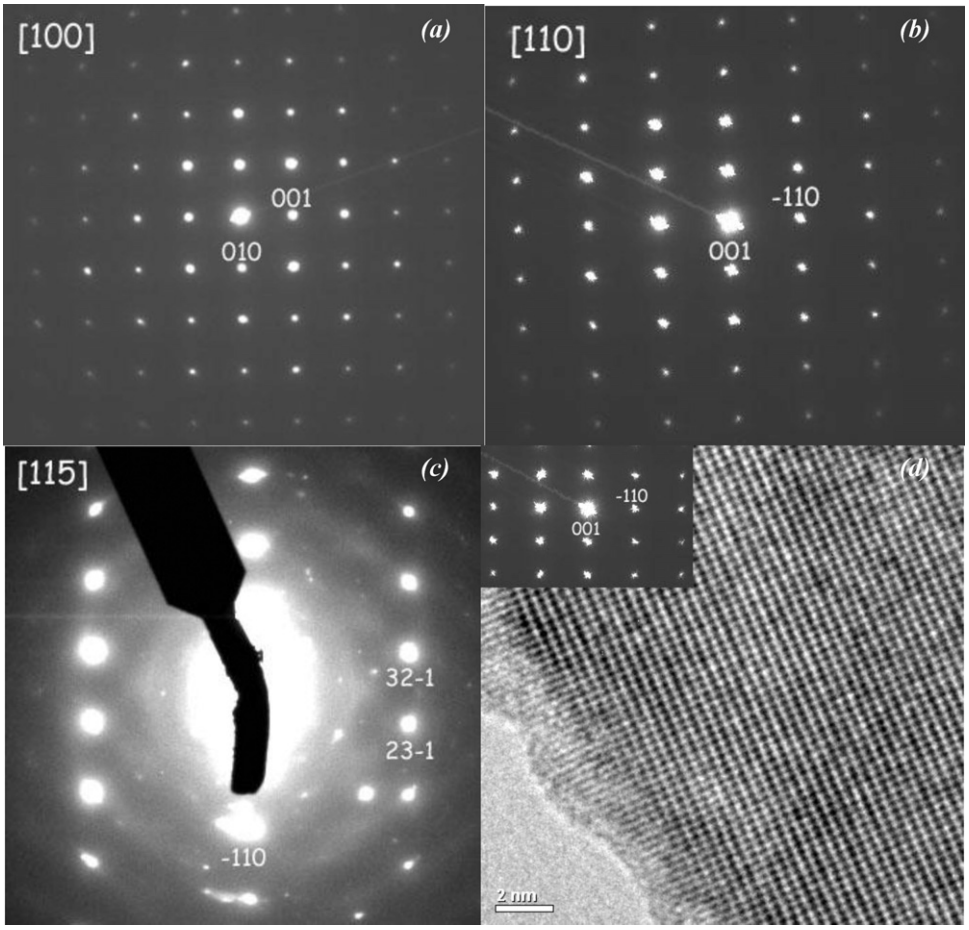


**Fig. 2.** TEM study of $BaIn_{0.3}Ti_{0.1}Fe_{0.6}O_{3-\delta}$: (a) [1 0 0] SAED pattern; (b) [1 1 0] SAED pattern; (c) [1 1 5] SAED pattern and (d) [1 1 0] HREM image of $BaIn_{0.3}Ti_{0.1}Fe_{0.6}O_{2.85-\delta}$.

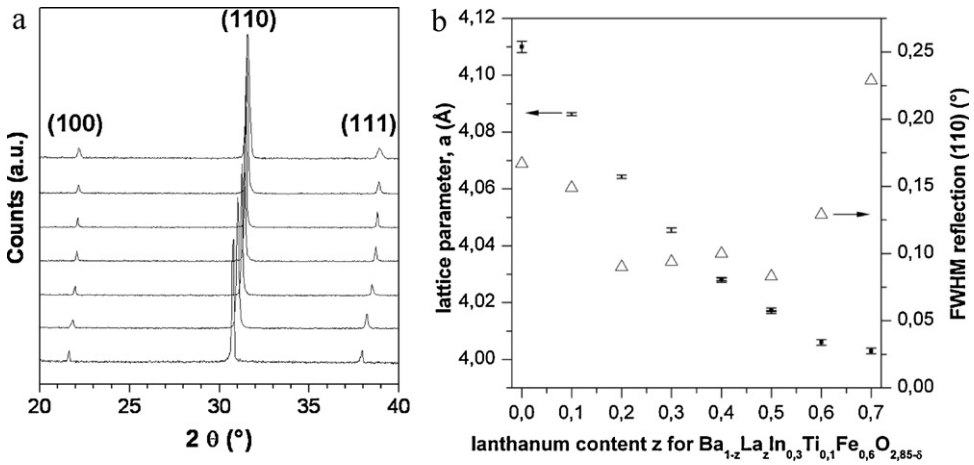


**Fig. 3.** (a) XRD patterns of $Ba_{1-z}La_zIn_{0.3}Ti_{0.1}Fe_{0.6}O_{3-\delta}$ with $0 \le z \le 0.7$ under air at RT and (b) lattice parameter and FWHM of the (1 1 0) reflection vs lanthanum content.

cation $La^{3+}$ ($r_e = 1.16$ Å) induces a cell parameter decrease. For $0.5 \le z \le 0.7$ a broadening of the diffraction peaks is observed once more.

Mössbauer spectrometry was used to determine the average valence of iron in these materials. $^{57}Fe$ Mössbauer spectra of $Ba_{1-y}La_yIn_{0.3}Ti_{0.1}Fe_{0.6}O_{3-\delta}$ compounds were first performed at 77 and 300 K with a large velocity scale to check that neither $Fe^{2+}$ nor Fe magnetic species occur. As illustrated in Fig. 4, the Mössbauer spectra obtained at 300 K (which are similar to those at 77 K) clearly exhibit quadrupolar structures. Each spectrum has to be fitted by means of at least three quadrupolar components. It is important to emphasize that due to the lack of resolution, different descriptions can be *a priori* proposed but a critical examination of these solutions and their evolution as a function of La substitution at both 300 K and 77 K allows to conclude to the fitting model which is now discussed. The corresponding hyperfine parameters of each doublet are listed in Table 1. According to the values of isomer shift, one distinguishes a quadrupolar component typical of a high-spin Fe(IV) ($-0.13 < \delta < -0.04$ mm s$^{-1}$) and the two others doublets characteristic of high-spin Fe(III) ($0.25 < \delta < 0.34$ mm s$^{-1}$), while their respective proportions directly result from the absorption areas, assuming the same Debye recoilless factor values. One observes that the mean values of isomer shift and those of Fe(IV) tend to increase when the La content increases while those of Fe(III) sites remain rather composition independent. An increase of the isomer shift might be explained by an increase of Fe(IV) bond valence, linked to a decrease of distance between $BO_6$ octaedra with reduction of A-site size. Moreover, quadrupolar splitting for Fe(IV) tends to decrease with lanthanum content. That gives information on a more regular environment, and may be linked to the decrease of the vacancy content.

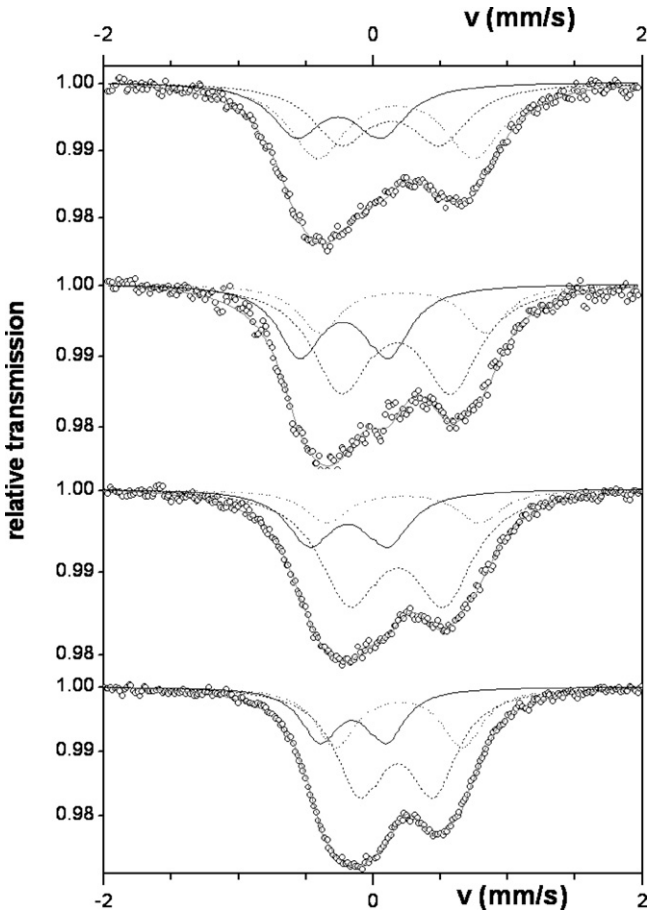


**Fig. 4.** Mössbauer spectra under air at 300 K of $Ba_{1-z}La_zIn_{0.3}Ti_{0.1}Fe_{0.6}O_{3-\delta}$ for $0.1 \le z \le 0.7$. Open circles correspond to experimental data, solid line to $Fe^{4+}$ fit; dash line to $^1Fe^{3+}$; dot line to $^2Fe^{3+}$ and grey solid line to sum fitted spectrum.

The Mössbauer parameters of the Fe(III) sites are similar to those found for other strongly oxygen-deficient materials as $SrFeO_{3\pm y}$ [12–14] and $SrFe_{1\pm x}Ti_xO_{3\pm y}$ [15–18]. The evaluation of Fe(III) environments is more difficult than those of Fe(IV). As previously reported, Fe(IV) tends to accept octahedral site. It would also be possible to assume that the highest isomer shift, close to 0.34 mm s$^{-1}$, coupled with high quadripolar splitting value, would correspond to the octahedral environment for Fe(III). For the second contribution ($\delta \sim 0.25$ mm s$^{-1}$), coordination would be lower than 6-fold because of lower isomer shift than octahedral values.

Integration of simulated area shows that the quantity of Fe(IV) has slowly decreased (25–21%) with the increase of lanthanum content in compounds. Substitution of $Ba^{2+}$ by $La^{3+}$ leads to a slightly decrease of lower mean valence for iron. Therefore, the substitution of barium by lanthanum might have a higher effect on the diminution of vacancies content (see Table 1). For $z = 0.7$, the oxygen content is close to the maximum value for a cubic perovskite structure. For higher lanthanum content, compounds would exhibit an excess of non-stoichiometric oxygen.

### 3.3. Electrical conductivity

The Arrhenius plots of electrical conductivity of $BaIn_{0.3}Ti_{0.7-y}Fe_yO_{3-\delta}$ ($y = 0$, 0.2 and 0.4) and

**Table 1**
Mössbauer parameters (isomer shift $\delta$, quadrupolar splitting $\Delta E$, proportions $p$) of each doublet of $Ba_{1-z}La_zIn_{0.3}Ti_{0.1}Fe_{0.6}O_{3-\delta}$ spectra and linked oxygen stoichiometry.

| $z$ | Valence | $\delta$ (mm s$^{-1}$) ± 0.02 | $\Delta E$ (mm s$^{-1}$) ± 0.02 | $p$ (%) ± 2 | Oxygen stoichiometry |
|---|---|---|---|---|---|
| 0.1 | $Fe^{III}$ | 0.29 | 1.14 | 42 | 2.68 |
| | $Fe^{IV}$ | 0.25 | 0.72 | 33 | |
| | | −0.13 | 0.61 | 25 | |
| 0.3 | $Fe^{III}$ | 0.34 | 1.21 | 18 | 2.78 |
| | $Fe^{IV}$ | 0.29 | 0.80 | 54 | |
| | | −0.09 | 0.64 | 28 | |
| 0.5 | $Fe^{III}$ | 0.34 | 1.12 | 14 | 2.87 |
| | $Fe^{IV}$ | 0.29 | 0.68 | 63 | |
| | | −0.06 | 0.56 | 23 | |
| 0.7 | $Fe^{III}$ | 0.32 | 0.92 | 26 | 2.93 |
| | $Fe^{IV}$ | 0.29 | 0.53 | 53 | |
| | | −0.04 | 0.48 | 21 | |

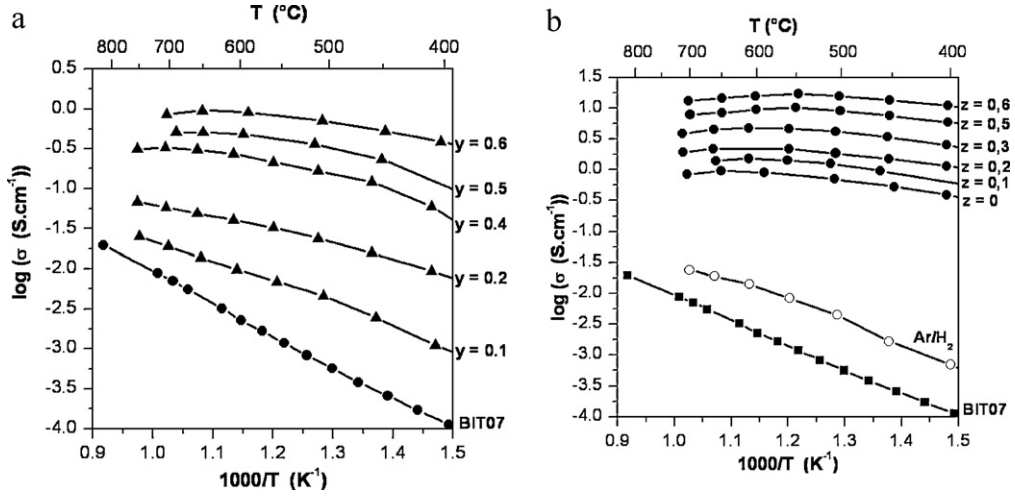


**Fig. 5.** DC conductivity vs. temperature for (a) $BaIn_{0.3}Ti_{0.7-y}Fe_yO_{2.85-\delta}$ compounds ($0 \le y \le 0.6$) under air and (b) $Ba_{1-z}La_zIn_{0.3}Ti_{0.1}Fe_{0.6}O_{3-\delta}$ compounds ($0 \le z \le 0.6$) under air (black symbol) and $z = 0.3$ under$Ar/H_2$ (5%) (open circle).

$Ba_{1-z}La_zIn_{0.3}Ti_{0.1}Fe_{0.6}O_{3-\delta}$ ($z = 0.1$, 0.2 and 0.3) materials are shown in Fig. 5. The conductivity curves under air exhibit a maximum towards 550–600 °C, due to the partial reduction with temperature of $Fe^{4+}$ into $Fe^{3+}$.

For low Fe contents, the temperature dependence of the electrical conductivity indicates a semiconducting behaviour which changes into pseudo metallic one when $y$ exceeds 0.4. Furthermore, the total conductivity increases significantly with the Fe and La content, at least 2 orders of magnitude. Thus, $BaIn_{0.3}Ti_{0.7}O_{3-\delta}$ (BIT07) yields a conductivity of $10^{-2}$ S cm$^{-1}$ at 700 °C whereas $Ba_{0.7}La_{0.3}In_{0.3}Ti_{0.1}Fe_{0.6}O_{3-\delta}$ (BLITFe06) shows a conductivity of 3 S cm$^{-1}$. Activation energies of BLITFe06 compounds are quite similar i.e. $E_a \approx 0.3$ eV. BITFe and BLITFe are p-type conductors. In reducing atmosphere (Ar/5% $H_2$) their electrical conductivity decreases drastically due to the iron reduction which implies a decrease in the number of charge carriers. All compounds exhibit similar temperature dependence of conductivity and a significant increase in the activation energy is also observed ($E_a \approx 0.6$ eV). The best conductivity at 700 °C ($2 \times 10^{-2}$ S cm$^{-1}$) was obtained for $Ba_{0.7}La_{0.3}In_{0.3}Ti_{0.1}Fe_{0.6}O_{3-\delta}$ (see Fig. 5(b)). $Fe^{4+}$ into $Fe^{3+}$ reduction was confirmed by temperature-programmed reduction (TPR). Indeed, as illustrated in Fig. 6, the peak at $T \approx 400$ °C can be assigned to iron reduction. The consumption of hydrogen measured indicates a decrease of the mean iron valence from 3.3 to 3. Moreover, no extra reduction peaks were observed up to 750 °C, attesting the redox stability of this material under reducing atmosphere.

Due to their low electrical conductivity at low $pO_2$, these materials can not be used as MIEC anodes; however they can be used as cermet components. Because $Ba_{0.7}La_{0.3}In_{0.3}Ti_{0.1}Fe_{0.6}O_{3-\delta}$ shows the best conductivity at 700 °C in air and under Ar/5%$H_2$, it was retained for cermets elaboration.

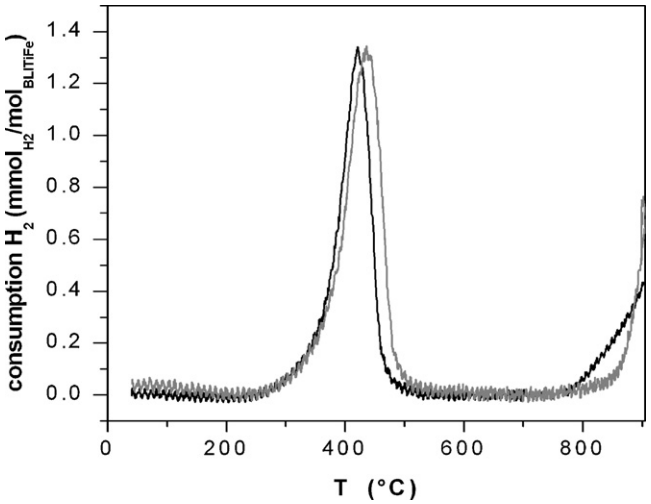


**Fig. 6.** Normalized TPR profile of $Ba_{0.7}La_{0.3}In_{0.3}Ti_{0.1}Fe_{0.6}O_{3-\delta}$ (black) and $Ba_{0.7}La_{0.3}In_{0.3}Ti_{0.1}Fe_{0.6}O_{3-\delta}$ (light grey).

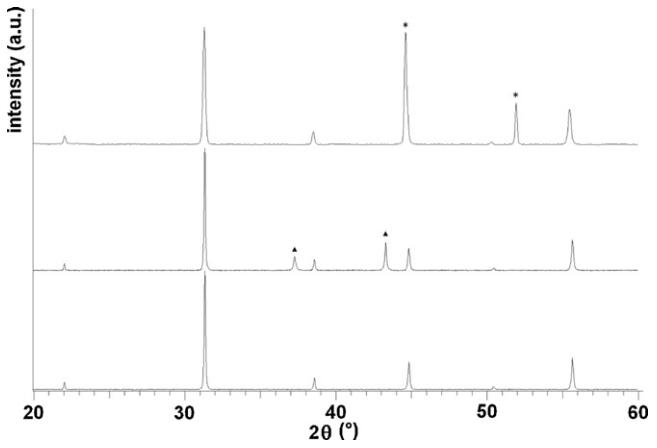


**Fig. 7.** XRD patterns of (a) $Ba_{0.7}La_{0.3}In_{0.3}Ti_{0.1}Fe_{0.6}O_{3-\delta}$; (b) $NiO/Ba_{0.7}La_{0.3}In_{0.3}Ti_{0.1}Fe_{0.6}O_{3-\delta}$; (c) $Ni/Ba_{0.7}La_{0.3}In_{0.3}Ti_{0.1}Fe_{0.6}O_{3-\delta}$; (*) Ni reflections and (▲) NiO reflections.

### 3.4. The $Ni/Ba_{0.7}La_{0.3}In_{0.3}Ti_{0.1}Fe_{0.6}O_{3-\delta}$ cermets

As mentioned before Ni/BIT07 cermets containing 18.7 vol.% of nickel (30 wt.% of NiO) exhibit promising characteristics for anode applications [4]. In order to easier compare these cermets to those based on BLITFe06, several NiO/BLITFe06 weight ratios were considered: a ratio equivalent to that of Ni/BIT07 cermets (30/70 wt%), a higher ratio 40/60 and an inferior one 25/75. These weight ratios correspond to a volumetric percentage of nickel of 19.8, 27.7 and 16.1 respectively. The Ni/BLITFe06 cermets were prepared as described in experimental section. The XRD pattern corresponding to 70/30 cermet is shown in Fig. 7 as example. The thermal treatment does not induce any chemical reaction between constituents. This feature was confirmed by a refinement of cubic cell parameter of $Ba_{0.7}La_{0.3}In_{0.3}Ti_{0.1}Fe_{0.6}O_{3-\delta}$ by full pattern matching, indicating no change with respect to the initial value. At this stage, the density reaches $75 \pm 2\%$ theoretical density. Finally, rectangular shaped samples were subjected to a reducing process for 5 h at 750 °C under flowing wet $Ar/H_2$ (5%).The weight loss observed during TG analysis of $Ba_{0.7}La_{0.3}In_{0.3}Ti_{0.1}Fe_{0.6}O_{3-\delta}$/NiO mixtures under these reducing conditions (see Fig. 8) corresponds to a complete reduction of NiO to Ni. An extra weight loss of 0.6% related to reduction

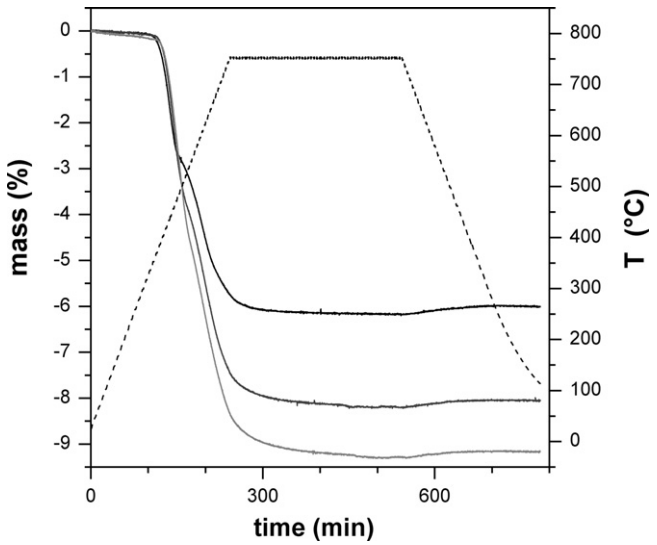


**Fig. 8.** TG curves under wet 5% $H_2$/Ar of NiO/BLITFe06 with different wt.% of NiO: (a) 25%, (b) 35% and (c) 40%.

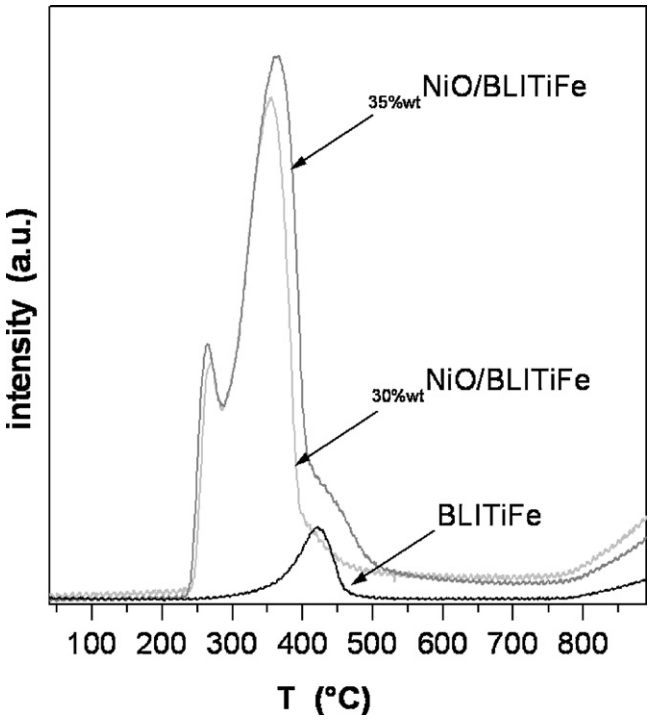


**Fig. 9.** Normalized TPR of $Ba_{0.7}La_{0.3}In_{0.3}Ti_{0.1}Fe_{0.6}O_{3-\delta}$ and nickel-based cermets with 30 wt.% and 35 wt.% of NiO.

of $Fe^{4+} \rightarrow Fe^{3+}$ was also observed In fact, iron reduction is accompanied by an oxygen loss to preserve the electroneutrality of BLITFe06. No impurity was detected in the XRD of the Ni/BLITFe06 cermets thus prepared. The reduction step does not induce any measurable further shrinkage of the samples. Therefore, due to oxygen loss, the density decreases down to 60% that is overall porosity reaches 40%. Moreover, the reducibility of the perovskite does not seem to be affected by the presence of nickel contrary to what described before for other perovskites [19,20]. As shown in Fig. 9, the temperature of iron reduction does not depend on the nickel content in the cermet. For BLITFe, only one peak of $H_2$ consumption is observed in the TPR. This peak between 350 °C and 450 °C is associated to $Fe^{4+} \rightarrow Fe^{3+}$ reduction. In the case of cermets, three peaks of $H_2$ consumption are observed between 230 °C and 500 °C. The two most intense peaks, localized between 265 °C and 370 °C, are related to nickel reduction. The intensity of iron reduction peak remains very weak compared to those of NiO reduction because the oxygen amount released in both processes is quite different. The intensity of NiO reduction peaks increases logically with the nickel rate.

### 3.5. Thermal expansion behaviour

Concerning the mechanical properties of the anodes, the thermal expansion coefficient (TEC) is a key factor for manufacturing cells. Thus, the TEC of BLITFe0.6 was inferred from the relative evolution of the cubic cell parameter vs. temperature between RT and 700 °C (see Fig. 10). The TEC corresponds to the slope of the linear function $\Delta a/a_0 = F(T)$. Its value ($TEC \sim 22(1) \times 10^{-6}\,K^{-1}$) fairly agrees with those generally obtained for ferrites [21,22] but is rather different from that of BIT07 ($TEC = 9.9 \times 10^{-6}\,K^{-1}$). For Ni/BLITFe0.6 cermets, the TEC was first calculated from the volume fraction ($\alpha_i$), the elastic modulus ($E_i$) and $TEC_i$ of each constituent according to the formula [23]:

$$TEC_{cermet} = \frac{\alpha_m\,TEC_m E_m + \alpha_c\,TEC_c E_c}{TEC_m E_m + TEC_c E_c}$$

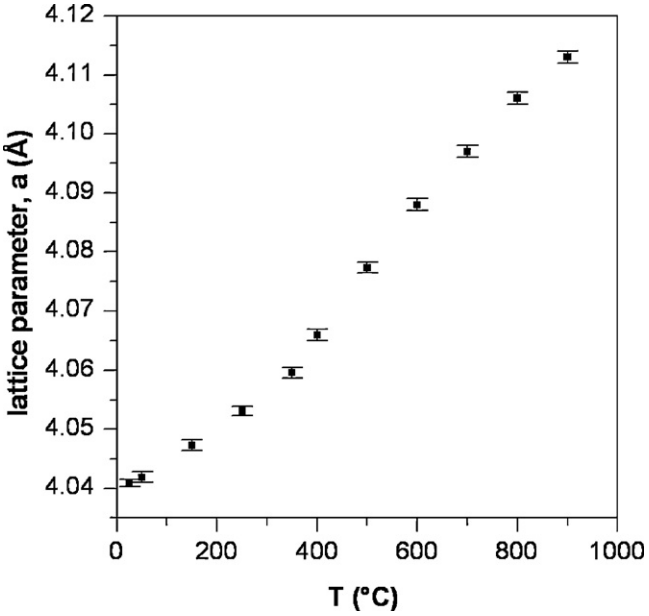


**Fig. 10.** Temperature dependence of lattice parameters of $Ba_{0.7}La_{0.3}In_{0.3}Ti_{0.1}Fe_{0.6}O_{3-\delta}$ in the range of 25–900 °C.

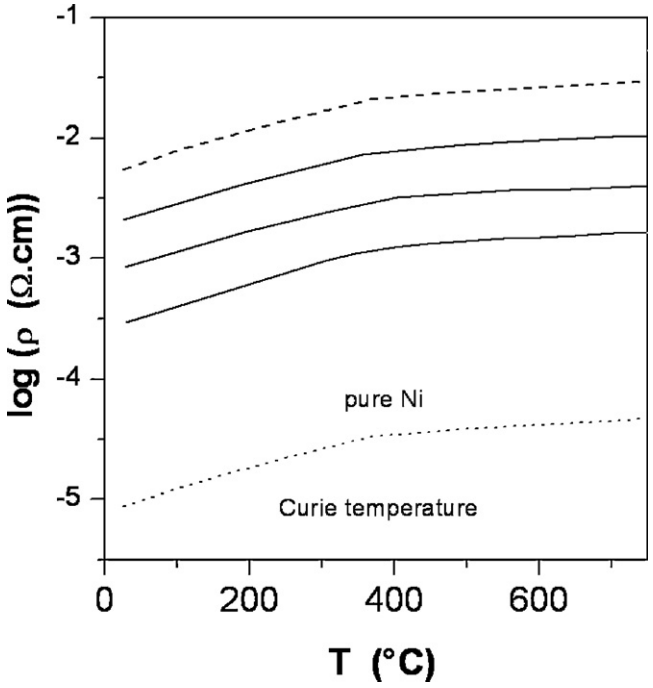


**Fig. 11.** Conductivity data for (a) pure Ni; (b) 27.7 vol.% Ni/BLITFe; (c) 19.8 vol.% Ni/BLITFe; (d) 16.1 vol.% Ni/BLITFe; (e) 18.7 vol.% Ni/BIT07.

where indices m and c refer to Ni and BLITFe06 respectively ($TEC_m = 13.5 \times 10^{-6}\,K^{-1}$, $E_m = 197$ GPa and $TEC_c = 22 \times 10^{-6}(1)\,K^{-1}$). Since the value of $E_c$ is not established it was assumed equal to $E_{BaTiO_3} = 67$ GPa). The values of TEC thus estimated for various cermets are listed in Table 2.

### 3.6. Influence of the Ni content on the DC conductivity of the cermets

DC conductivity measurements were carried out between RT and 700 °C under Ar/5% $H_2$ on Ni/$Ba_{0.7}La_{0.3}In_{0.3}Ti_{0.1}Fe_{0.6}O_{3-\delta}$ cermets with various Ni contents (27.7, 19.8 and 16.1 vol.%). The total DC resistivity values were then compared to data reported for pure nickel [24] and a 18.7 vol.% Ni/BIT07 cermet [4]. In Fig. 11, a sharp change in slope can be observed for all the curves in correspondence to the Curie temperature of Ni (at 350 °C). The increase in resistivity with increasing temperature indicates a metallic behaviour. Interestingly, the electronic conductivity of each Ni/BLITFe-type cermets is higher than that of 18.7 vol.% Ni/BIT07 ($\sigma_{700\,°C} \approx 10^2\,S\,cm^{-1}$), even for a lower Ni content (16.1 vol.% Ni/BLITFe06 $\sigma_{700\,°C} \approx 200\,S\,cm^{-1}$). As expected, the conductivity of Ni/BLITFe06 cermets increases with Ni rate. The best results were obtained for 27.7 vol.% Ni/BLITFe06 cermet with $\sigma_{700\,°C} \approx 1000\,S\,cm^{-1}$. The same level of conductivity was obtained for a 30 vol.% Ni/YSZ cermet [25].

In order to determine the percolation threshold, i.e. the Ni content for which a sharp drop in electronic conductivity is observed, several Ni/BLITFe06 cermets with decreasing Ni contents were prepared and subjected to DC conductivity measurements at RT. It is important to emphasize that the conductivity of the cermets as a function of the nickel content (Fig. 12) shows the S-shaped curve predicted by percolation theory [26]. It leads to a percolation threshold ranged between 9% and 11 vol.% of Ni. This value is significantly lower than that reported for Ni/BIT07 cermets (15.7 vol.%) [4] and than values derived from numerical simulations for disordered 3D systems (14.5 vol.%) [27–29]. This feature could be related with the specific microstructure of Ni/BLITFe06 cermets. Actually, as described by Da He et al. [30] the grain size ratio of insulating to conductive powders (λ) influences significantly the conductive percolation threshold which decreases when λ increases. As illustrated in Fig. 13, the grain size ratio BLITFe06/Ni is appreciably higher than

**Table 2**
Calculated TECs of Ni/BLITFe06 cermets.

| Ni (vol.%) | Calculated TEC ($\times 10^{-6}\,K^{-1}$) |
|---|---|
| 5 | 20.9 |
| 10 | 19.9 |
| 15 | 19.1 |
| 20 | 18.4 |
| 25 | 17.8 |
| 30 | 17.3 |
| 40 | 16.4 |

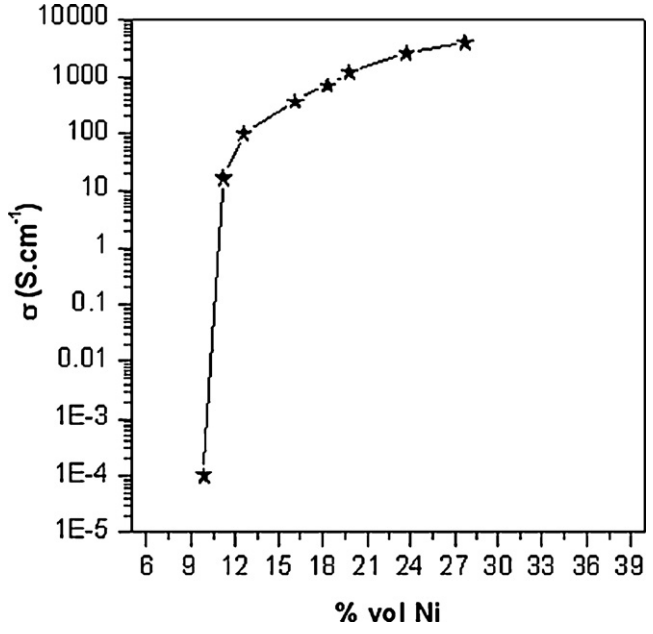


**Fig. 12.** Ni (vol.%) dependence of total conductivity of Ni/BLITFe cermets at 25 °C.

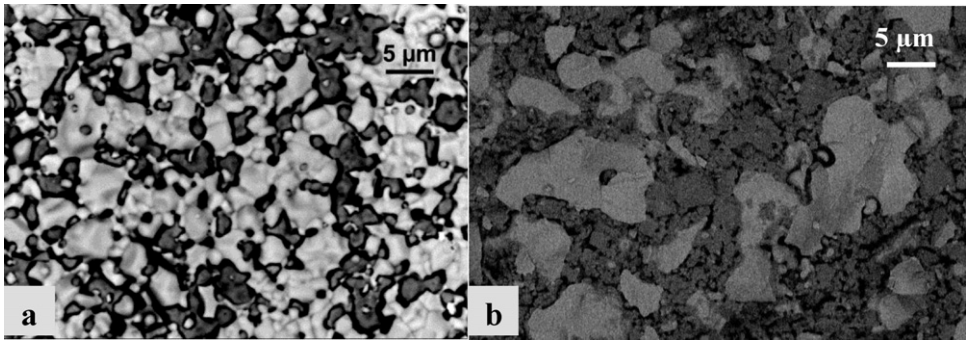


**Fig. 13.** SEM micrographs of (a) Ni/BIT07 and (b) Ni/BLITFe06.

the BIT07/Ni one. In fact, BIT07 and BLITFe06 exhibit a sintering behaviour quite different which can explain this feature. A large value of λ avoids small particles to be isolated in the regions occupied by the large particles. Thus, for the Ni/BLITFe06 cermet, one can observe the formation of large clusters of Ni to span the packing structure. This leads to a decrease of the percolation threshold which moves favourably towards the small quantities of nickel.

### 3.7. Electrochemical characterization

The electrochemical behaviour of Ni/BIT07 and Ni/BLITFe06 cermets was studied by EIS. In order to facilitate comparison with previous results [5] a content of NiO equal to 40 wt% was used to elaborate cermets. Symmetrical cells of Ni/BIT07//BIT07//Ni/BIT07 and Ni/BLITFe06//BIT07//Ni/BLITFe06 were prepared by tape casting and co-sintering as described in Section 2.

EIS measurements were performed between 400 and 700 °C under 5% $H_2$/95% Ar and methane both humidified. Fig. 14 shows the impedance diagrams of the symmetrical cells at 400 °C. The experimental data were analyzed, using the Zview® software (Scribner Associates). The best equivalent circuit fitting comprises a series of three parallel combinations of resistance and a constant phase element, CPE. The first contribution, in the high frequency range, is attributed to the BIT07 electrolyte. All the impedance diagrams reveal the presence of two semi-circles associated to the electrode responses; describing the two processes that contribute to the electrode/electrolyte interface impedance. For these samples, at high temperature (>500 °C), an additional phenomena is observed at high frequency in the Nyquist diagrams. An inductive component ($L$) is taken into account and added in series to the corresponding equivalent circuit (Fig. 15). The inductance $L$ is ascribed to the leads and the resistance of electrolyte in this case is calculated by the intercept with real-axis ($R_1$). The polarization resistance of the electrode, $R_p$, represents the sum of resistances $R_2$ and $R_3$.

The area specific resistance (ASR) was calculated multiplying $R_p$ by the surface of cathode (~0.3 $cm^2$) all divided by 2 since the cell is symmetrical. As shown in Table 3, under wet hydrogen, the symmetrical cell with Ni/BLITFe06 anode has an ASR values smaller than that of the symmetrical cell with Ni/BIT07. At 700 °C, an ASR of 0.2 Ω $cm^2$ is obtained which is noticeably inferior to that measured for symmetrical cells based on Ni/BIT07 (1.7 Ω $cm^2$).

This improvement results from the increased of the oxygen ionic conducting phase which can increase the triple phase boundary zone and/or the electrocatalytic activity of the material.Under

**Table 3**
The ASR values of symmetrical cells of Ni/BLTIFe06 and Ni/BIT07 anode on BIT07 electrolyte obtained under wet $H_2$ and $CH_4$.

| Temperature (°C) | ASR (Ω $cm^2$) | | |
|---|---|---|---|
| | Ni–BIT07/BIT07 under wet $H_2$/Ar | Ni–BLITFe06/ BIT07 under wet $H_2$/Ar | Ni–BLITFe06/BIT07 under wet $CH_4$/Ar |
| 700 | 1.7 | 0.2 | 0.6 |
| 600 | 5.8 | 0.7 | 1.7 |
| 500 | 11.6 | 1.3 | 4.4 |
| 400 | 14.3 | 13.4 | 44.2 |

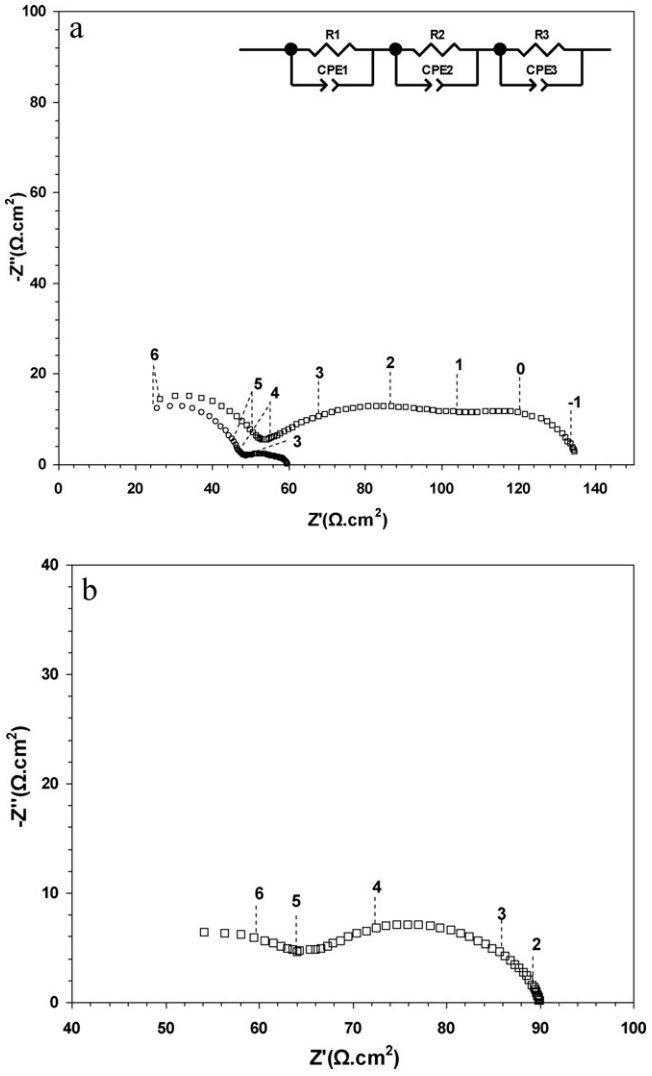


**Fig. 14.** Nyquist impedance diagrams at 400 °C of (a) Ni–BLITFe06/BIT07/Ni–BLITFe06; (b) Ni–BIT07/BIT07/Ni–BIT07 symmetrical cell in wet Ar/$H_2$ (circles) and wet $CH_4$ (squares). Frequency logarithms are indicated.

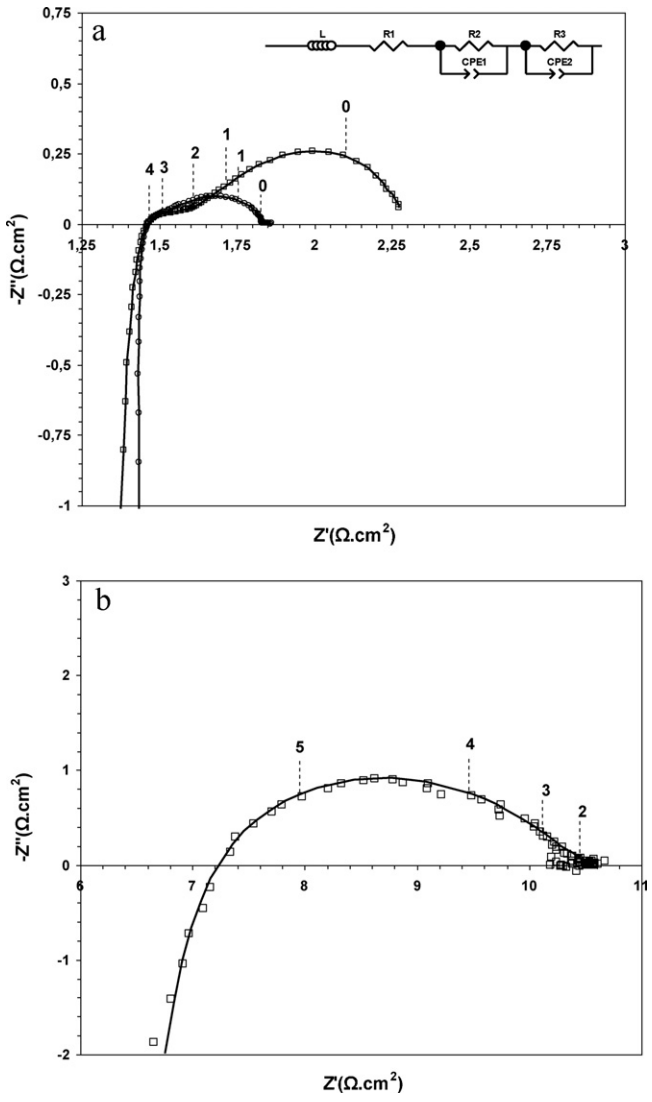


**Fig. 15.** Nyquist impedance diagrams at 700 °C of (a) Ni–BLITFe06/BIT07/Ni–BLITFe06; (b) Ni–BIT07/BIT07/Ni–BIT07 symmetrical cell in wet $Ar/H_2$ (circles) and wet $CH_4$ (squares). Points are experimental data and lines are fit data with the equivalent circuit. Frequency logarithms are indicated.

wet methane, the frequency ranges associated with the electrochemical processes are similar to that obtained under wet $H_2$; two semi-circles are observed at medium and low frequencies in the Nyquist diagrams (Fig. 15(a)). Nevertheless, the ASR increases up to $0.6\,\Omega\,cm^2$, but remains compatible with the SOFC target values. However, for Ni/BIT07 no electrochemical measurement could be made because the symmetrical cells were destroyed as consequence of coking phenomenon. In the case of Ni/BLITIFE carbon deposition is also observed as indicates the blackening of the symmetrical cells and the weak increase of their diameter after EIS measurements. However, the mechanical resistance of the cell is still good what seems to indicate that coking is less important.

## 4. Conclusion

A new family of MIEC compounds resulting from the electrolyte BIT07 was developed by the coupled substitution Fe → Ti and La → Ba. The total conductivity increases significantly with the Fe and La content, at least 2 orders of magnitude. $BaIn_{0.3}Ti_{0.7}O_{3-\delta}$ (BIT07) yields a total conductivity in air of $10^{-2}\,S\,cm^{-1}$ at 700 °C whereas that of $Ba_{0.7}La_{0.3}In_{0.3}Ti_{0.1}Fe_{0.6}O_{3-\delta}$ (BLITFe06) is estimated at $3\,S\,cm^{-1}$. However, under reducing atmosphere, the best level of conductivity obtained for the BLITFe compounds ($2\times10^{-2}\,S\,cm^{-1}$) is not sufficient for a use as MIEC anode. On the contrary, Ni/BLITFe06 cermets exhibit the level of conductivity required for SOFC device. The electronic conductivity of Ni/BLITFe06 cermet is higher than that of Ni/BIT07 cermet even for Ni a lower content. Moreover, the percolation threshold moves favourably towards the small quantities of nickel. Finally, Ni/BLITFe06 cermets show a better electrochemical behaviour towards fuel oxidation. However, an optimization of the electrode microstructure aiming to decrease the quantity of nickel, thus a complete study of the average contributions and low frequencies of the diagrams of impedance, must be made to still improve resistance to coking of these anodes.

## Acknowledgements

The authors thank Dr Alain Thorel for helpful discussions and Dr Marika Letilly for her advice on tape casting process. The European Institute for Energy Research (EifER) and the Agence de l'Environnement et de la Maîtrise de l'Energie (ADEME) are also thanked for the PhD fellowship awarded to F. Moser.

## References

[1] E.V. Tsipis, V.V. Kharton, J. Solid State Electrochem. 12 (2008) 1039–1060.
[2] J.W. Fergus, J. Power Sources 162 (2006) 30–40.
[3] V. Jayaraman, A. Magrez, M.T. Caldes, O. Joubert, M. Ganne, Y. Piffard, L. Brohan, Solid State Ionics 170 (2004) 17–24.
[4] T. Delahaye, O. Joubert, M.T. Caldes, Y. Piffard, P. Stevens, Solid State Ionics 177 (2006) 2945–2950.
[5] D. Prakash, T. Delahaye, O. Joubert, M.T. Caldes, Y. Piffard, J. Power Sources 167 (2007) 111–117.
[6] J.B Goodenough, Y.H. Huang, J. Power Sources 173 (2007) 1–10.
[7] S. Tao, J.T.S. Irvine, J. Electrochem. Soc. 151 (2) (2004) A252–A259.
[8] J. Liu, B. Madsen, Z. Ji, S. Barnett, Electrochem. Solid-State Lett. 5 (6) (2002) A122–A124.
[9] Y.H. Huang, R.I. Dass, J.C. Denyszyn, J.B. Goodenough, J. Electrochem. Soc. 153 (7) (2006) A1266–A1272.
[10] S. Hamakawa, K. Sato, T. Inoue, M. Nishioka, K. Kobayashi, F. Mizukami, Catal. Today 117 (2006) 297–303.
[11] T. Roisnel, J. Rodriguez-Carjaval, Physica B 192 (1993) 55, See also http://www-llb.cea.fr/fullweb/fp2k/fp2k.htm.
[12] T.C. Gibb, J. Chem. Soc. Dalton Trans. (1985) 1455–1470.
[13] Y. Takeda, K. Kanno, T. Takada, O. Yamamoto, M. Takano, N. Nakayama, Y. Bando, J. Solid State Chem. 63 (1986) 237–249.
[14] M. Takano, T. Okita, N. Nakayama, Y. Bando, Y. Takeda, O. Yamamoto, J.B. Goodenough, J. Solid State Chem. 73 (1988) 140–150.
[15] C. Greaves, R.A. Buker, Mater. Res. Bull. 21 (1986) 823–833.
[16] J. Rodriguez, J.A. Pereda, M. Vallet, J.G. Calbet, J. Tejada, Mater. Res. Bull. 21 (1986) 255–263.
[17] T.C. Gibb, P.D. Battle, S.K. Bollen, R.J. Whitehead, J. Mater. Chem. 2 (1992) 111–114.
[18] P. Adler, S. Eriksson, Z. Anorg. Allg. Chem. 626 (2000) 118–124.
[19] J. Bonn, F.P.F. van Berkel, E.R. Stobbe, 15th World Hydrogen Energy Conference, Yokohama, Japan, 2004.
[20] E. Ruckenstein, H.Y. Wang, J. Catal. 187 (1999) 151–159.
[21] F. Prado, L. Mogni, G.J. Cuello, A. Caneiro, Solid State Ionics 178 (2007) 77–82.
[22] A. Mai, Vincent, A.C. Haanappel, S. Uhlenbruck, F. Tietz, D. Stöver, Solid State Ionics 176 (2005) 1341–1350.
[23] R.M.C. Clemmer, S.F. Corbin, Solid State Ionics 166 (2004) 251–259.
[24] H. Ullmann, N. Trofimenko, F. Tietz, D. Stöver, A. Ahmad-Khanlou, Solid State Ionics 138 (2000) 79–90.
[25] M.H. Pihlatie, A. Kaiser, M. Mogensen, M. Chen, Solid State Ionics 189 (2011) 82–90.
[26] J.P. Clerc, G. Giraud, J. Roussenq, R. Blanc, J.P. Caron, E. Guyon, H. Ottav, D. Stauffer, Ann. Phys. Fr. 8 (1983) 1.
[27] I. Webman, J. Jortner, M.H. Cohen, Phys. Rev. B 11 (1975) 2885–2892.
[28] I. Webman, J. Jortner, M.H. Cohen, Phys. Rev. B 16 (1977) 2593–2596.
[29] M.H. Cohen, J. Jortner, I. Webman, AIP Conf. Proc. 40 (1978) 63.
[30] D. He, N.N. Ekere, J. Phys. D: Appl. Phys. 37 (2004) 1848–1852.